



Cite this: *RSC Adv.*, 2023, 13, 27212

# Insights into the evolution of chemical structure and pyrolysis reactivity of PVC-derived hydrochar during hydrothermal carbonization†

Ling Zhang,<sup>ab</sup> Qing Wang,<sup>ab</sup>  Faxing Xu<sup>c</sup> and Zhenye Wang<sup>c</sup>

Hydrothermal carbonization (HTC) is emerging as an effective technology to convert PVC into highly valuable materials via the removal of chlorine. This means that an in-depth understanding of HTC requires the hydrochar structure, thermal degradation behavior, and relationship between structure and thermal reactivity to be understood. In this work, two typical PVC waste materials were selected for HTC experiments at different temperatures. The structure of the hydrochar was characterized in detail by compositional analysis, FTIR spectroscopy, and <sup>13</sup>C NMR analysis. Furthermore, the thermal degradation behavior of the hydrochar was analyzed. The changes after thermal degradation were used to establish a correlation with pyrolysis reactivity. The results showed that the C content and chemical structure of the hydrochar approached that of bituminous coal with increasing HTC temperature. Compared with the untreated PVC feedstock, the hydrochar exhibited higher levels of oxygen-containing functional groups on its surface, and its carbon skeleton structure changed from polymeric straight chains to short-chain paraffins, cycloalkanes, and aromatics. A negative correlation was observed between the CPI value of the hydrochar derived from SPVC and the HTC temperature. The structural evolution path of the hydrochar was altered by additives, which improved its thermal reactivity. These findings are expected to play a significant role in bridging the gap from the creation of a theoretical potential energy source to the development of a sustainable alternative renewable fuel.

Received 24th July 2023  
Accepted 31st August 2023

DOI: 10.1039/d3ra04986h

rsc.li/rsc-advances

## 1. Introduction

The two major challenges facing mankind are environmental pollution and the energy crisis. PVC is the third most widely produced plastic resin. 43% of the PVC polymer mass is derived from petrochemical raw materials, and 57% comes from the chlorine atoms in sea salt.<sup>1</sup> Global PVC production is expected to reach 59.72 million tons by 2030.<sup>2</sup> In addition to further aggravating the energy crisis, the continuous accumulation of used PVC products in solid waste has contributed to an increase in chlorine levels.<sup>3</sup> Moreover, the treatment of chlorine-containing waste is a bottleneck for proper solid waste disposal and resource recovery.<sup>4</sup> However, in addition to being a waste material, PVC can be considered a valuable source of carbon materials and fuel because C makes up 92.3% of dechlorinated PVC.<sup>5,6</sup> The dual “resource” and “waste” properties of

PVC emphasize the importance of effective utilization methods for realizing energy recovery with no environmental pollution.

Traditional PVC waste recycling methods mainly include mechanical recycling, landfills, and incineration.<sup>7</sup> However, it is difficult to separate large amounts of PVC waste from solid waste because it is highly dispersed. More importantly, mechanically recycled products usually have lower values.<sup>8</sup> Landfilling is a simple and easy method with low disposal costs. However, plastics have high calorific value, meaning that landfilling is a huge waste of resources. In addition, it is difficult to decompose PVC, and land cannot be plowed for decades or even centuries after PVC is buried in the soil.<sup>9</sup> A major method for recovering heat is combustion with solid waste, but Cl is directly linked to the formation of dioxin, chlorination, and the evaporation of heavy metals.<sup>3</sup> Therefore, it is crucial to explore suitable technologies for the environmentally sound treatment and resource utilization of PVC waste.

Pyrolysis provides an eco-friendly disposal option that avoids the downsides of both incineration and landfill disposal.<sup>10</sup> Pyrolysis has garnered increased interest in the context of PVC disposal due to its potential to transform PVC into valuable commodities.<sup>11</sup> Gui *et al.* demonstrated that the yield of pyrolysis oil increased with increasing ultimate pyrolysis temperature. In the rapid pyrolysis of PVC, the yield increased from 6.13 wt% at 500 °C to 27.79 wt% at 800 °C.<sup>12</sup> Zhou *et al.* discovered that the products of the rapid pyrolysis of PVC

<sup>a</sup>Engineering Research Centre of Oil Shale Comprehensive Utilization, Ministry of Education, Northeast Electric Power University, Jilin City, Jilin, 132012, PR China. E-mail: rlx888@126.com

<sup>b</sup>Jilin Institute of Chemical Technology, Jilin City, Jilin, 132022, PR China

<sup>c</sup>Jilin Feite Environmental Protection Co. Ltd, Jilin Key Laboratory of Subcritical Hydrolysis Technology, Jilin, 132200, PR China

† Electronic supplementary information (ESI) available. See DOI: <https://doi.org/10.1039/d3ra04986h>



predominantly included aromatic hydrocarbons, olefins, hydrogen chloride, and chlorinated hydrocarbons (in order of decreasing proportion).<sup>13</sup> Zhou *et al.* employed thermal decomposition techniques to upgrade PVC into valuable carbon materials, pyrolysis gases suitable for pipeline utilization, and chloride compounds.<sup>14</sup> Xu *et al.* conducted the rapid pyrolysis of PVC artificial leather at 500 °C, obtaining an exceptionally high tar yield of 54.96 wt%.<sup>15</sup> However, the presence of chlorine in PVC results in the significant accumulation of residual chlorides within the pyrolysis products, which substantially diminishes product quality and constrains downstream applications.<sup>10,16</sup> Consequently, achieving the high-value utilization of PVC means that pre-pyrolysis dechlorination treatment is essential.

Hydrothermal carbonization (HTC) is an appealing technology for the valorization of biomass,<sup>17,18</sup> food waste,<sup>19</sup> municipal solid waste,<sup>20</sup> and sludge<sup>21</sup> into valuable carbon materials (hydrochar). In the context of sustainable development and environmental consciousness, HTC has garnered widespread attention due to its effective detoxification performance, particularly in the secure disposal of high halogen waste and energy recovery.<sup>16,22</sup> This technology is of significant interest due to its potential to fundamentally address the challenges associated with the large-scale transformation of PVC waste into low-chlorine solid products.<sup>5,23,24</sup> The organic chlorine in PVC is converted into easily recoverable water-soluble inorganic chlorine without generating dioxin (PCDD/Fs).<sup>25</sup> Moreover, high dechlorination efficiencies (DE) can be achieved at relatively mild temperatures. Both elimination and substitution reactions play an important role in the hydrothermal dechlorination of PVC.<sup>26,27</sup> By encouraging the substitution of  $-Cl$  with  $-OH$ , the addition of several alkaline and metal ions can lower the hydrothermal dechlorination temperature of PVC even further.<sup>6,28–30</sup> When PVC waste is carbonized by HTC, most of the original carbon tends to be preserved in the hydrochar, and the physicochemical qualities of this hydrochar are similar to those of natural coal.<sup>5</sup> In addition to its direct use in combustion, hydrochar can also be used as a precursor in pyrolysis or gasification processes to produce low-chlorine oil or hydrogen-rich gas.<sup>31–34</sup> Consequently, HTC is a promising technology for the pre-treatment and utilization of PVC waste, and the formed hydrochar is the key intermediate connecting PVC waste treatment with energy recovery.

Although much work has been done on the HTC treatment of PVC, most reported research has focused on the effects of operational parameters on PVC dechlorination and hydrochar fuel properties.<sup>5,6,35,36</sup> However, there are only a few studies evaluating the influence of hydrothermal temperature on the molecular structure and pyrolytic characteristics of solid products (hydrochars). The molecular structure and pyrolysis reactivity of hydrochars obtained under different hydrothermal temperatures are not yet clear. These factors are highly significant for the practical implementation of hydrothermal-pyrolysis technology in engineering applications.<sup>37</sup> Establishing the relationship between the molecular structure of hydrothermal carbons and their pyrolysis reactivity will contribute to a more

profound understanding of the thermal degradation mechanism of PVC.<sup>37–39</sup>

To address the knowledge gap in this domain, two types of PVC samples were hydrothermally treated within the temperature range of 220 °C to 260 °C in this work. The molecular structures of the obtained hydrochars were comprehensively characterized through elemental analysis, infrared spectroscopic (FTIR) analysis, and  $^{13}C$  nuclear magnetic resonance (NMR) spectroscopy. The structural parameters of the hydrochars were determined by peak fitting the  $^{13}C$  NMR spectra. Subsequently, thermogravimetric analysis was employed to assess the thermochemical reactivity of the hydrochar during the pyrolysis process. This study ultimately revealed the correlations between structural attributes and reactivity in the hydrochar pyrolysis process. These correlations provide a foundational understanding to discern the fundamental mechanism underlying the impact of hydrothermal treatment on PVC pyrolysis. The findings of this research contribute to a better understanding of the hydrothermal carbonization and copyrolysis treatment of PVC waste for resource utilization. This work offers valuable insights for devising and refining waste-to-energy strategies for PVC waste and serves as a practical reference for designing and optimizing such processes.

## 2. Material and methods

### 2.1. Materials

This investigation employed two distinct categories of PVC as source materials to represent PVC waste derived from industrial raw materials and household refuse. The first sample was PVC resin powder, also known as “SPVC,” which is a typical manufacturing waste product. The second sample was rigid PVC, also known as “RPVC,” which contains a variety of chemicals, including plasticizers, smoke suppressants, stabilizers, impact modifiers, processing aid resins, and fillers ( $CaCO_3$ ). The manufacturer of this sample did not provide precise composition details. Each sample was dried at 105 °C in a muffle furnace until a constant weight was achieved, pulverized to a particle size smaller than 2 mm, and stored in a hermetically sealed container for subsequent experimentation. A standard  $AgNO_3$  solution ( $1.0\text{ mol L}^{-1}$ ) was procured from Shenzhen Borinda Technology Co., Ltd.

### 2.2. Hydrothermal carbonization experiments

Fig. 1 depicts the HTC laboratory. Experiments were conducted in a 500 mL high-pressure reactor (HT-500FJ). According to previous studies, the hydrothermal temperature is a key factor affecting PVC dechlorination.<sup>23,40</sup> When the hydrothermal temperature exceeds 200 °C, PVC undergoes significant dechlorination and structural changes.<sup>28</sup> With a solid-liquid ratio of 1:10, hydrothermal temperature of 260 °C, and reaction time of 60 min, PVC is completely carbonized.<sup>5,25,41</sup> Therefore, 35 g of PVC sample and 350 mL of water were added to the reactor. Reaction temperatures of 220 °C, 240 °C, and 260 °C were used. The reaction time was set to 60 min and the stirring rate was  $200\text{ rpm min}^{-1}$ . These



are typical experimental conditions for the hydrothermal carbonization of PVC. To remove air from the reactor, high-grade nitrogen gas (99.9%) was sprayed on the piping and reactor for 10 min prior to each trial. The reaction time was defined as the amount of time that the reactor was held at the designated temperature, excluding preheating and cooling. After the reaction, the reactor was cooled to room temperature. Next, the solid and liquid components of the reaction mixture were separated using a vacuum suction filter. The solid residue was then washed under magnetic stirring until  $\text{AgNO}_3$  leaked into the cleaning liquid without turbidity. The cleaned solid was then dried to a constant mass at  $105^\circ\text{C}$  to obtain the hydrochar. Experiments were repeated three times. To characterize the solid samples, the solid products prepared under the same conditions were combined, ground to  $74\ \mu\text{m}$  or smaller particles, and stored in sealed bags. Each hydrochar was given the designation "X-XX", where, for example, S-240 stands for hydrochar prepared with SPVC treated at a temperature of  $240^\circ\text{C}$ .

## 2.3. Characterization of the samples

**2.3.1. Fundamental properties.** An elemental analyzer was used to determine the levels of C, H, N, and S in the samples. In accordance with EN14582:2007, oxygen bottle combustion ion chromatography was used to measure the chlorine concentration of the samples.<sup>42</sup> A completely automatic industrial analyzer was used to determine the proximate analysis. The difference technique was used to determine the fixed carbon (FC) and oxygen (O) fractions. An automated bomb calorimeter was used to determine higher heating values (Table 1). X-ray fluorescence (XRF) spectroscopy was used to evaluate the composition of RPVC, as listed in Table 2. The solid phase yield ratio was defined as shown in eqn (1) and the energy density was calculated according to eqn (2):

$$\text{Hydrochar yield} = \frac{M_1}{M_2} \times 100\% \quad (1)$$

where  $M_1$  is the weight of hydrochar after the HTC of SPVC or RPVC and  $M_2$  is the initial weight of SPVC or RPVC.

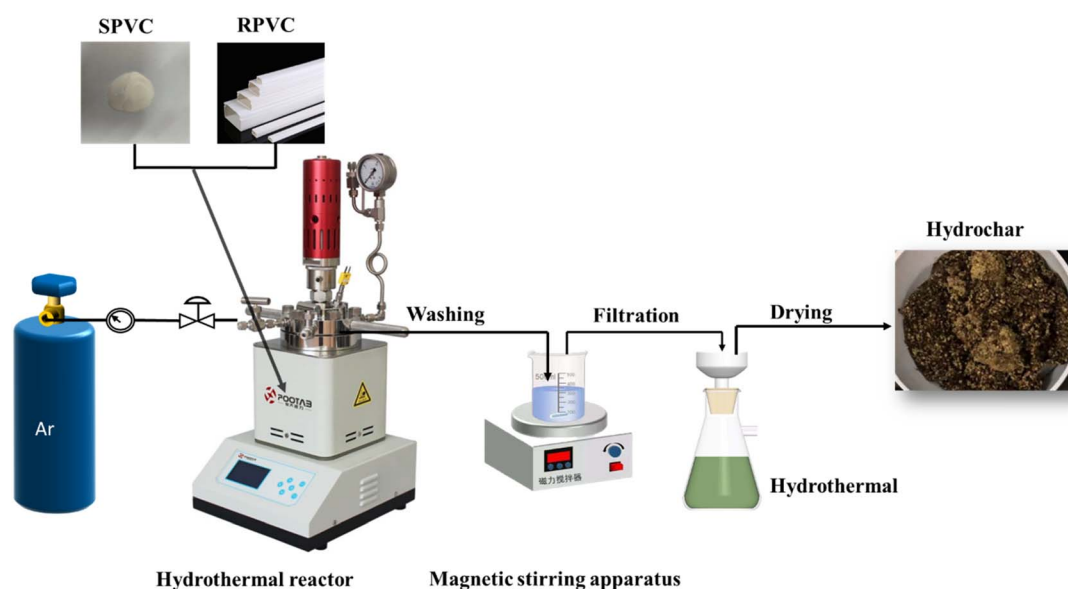


Fig. 1 Experimental hydrothermal carbonization setup.

Table 1 Experimental parameters and ultimate analysis for PVC resin and R-PVC<sup>b</sup>

Sample	Ultimate analysis (wt%, db)						Proximate analysis (wt%, db)			
	C	H	O <sup>a</sup>	S	N	Cl	V <sub>d</sub>	A <sub>d</sub>	FC <sup>a</sup>	HHV
SPVC	39.44 ± 0.24	6.73 ± 0.15	0.95 ± 0.32	<d.l.	<d.l.	52.88 ± 0.41	95.07 ± 0.42	0 ± 0.00	4.94 ± 0.18	20.05 ± 0.12
S-220	64.06 ± 0.31	7.18 ± 0.18	2.53 ± 0.34	<d.l.	<d.l.	24.15 ± 0.38	70.15 ± 0.38	2.09 ± 0.23	27.77 ± 0.12	26.04 ± 0.21
S-240	73.94 ± 0.42	7.52 ± 0.22	2.69 ± 0.42	<d.l.	<d.l.	11.07 ± 0.30	56.47 ± 0.51	4.78 ± 0.15	38.75 ± 0.21	29.22 ± 0.18
S-260	79.07 ± 0.36	6.68 ± 0.16	3.29 ± 0.31	<d.l.	<d.l.	5.20 ± 0.43	50.79 ± 0.44	5.76 ± 0.20	43.46 ± 0.17	35.04 ± 0.24
R-PVC	25.35 ± 0.36	3.10 ± 0.19	11.04 ± 0.38	0.17 ± 0.03	<d.l.	23.10 ± 0.46	48.68 ± 0.42	37.27 ± 0.51	14.05 ± 0.21	8.57 ± 0.19
R-220	24.99 ± 0.39	2.99 ± 0.17	8.31 ± 0.56	0.14 ± 0.04	<d.l.	20.05 ± 0.42	48.28 ± 0.37	43.58 ± 0.42	8.14 ± 0.32	8.14 ± 0.15
R-240	26.86 ± 0.43	3.14 ± 0.21	13.13 ± 0.49	0.14 ± 0.02	<d.l.	17.13 ± 0.31	52.08 ± 0.25	39.64 ± 0.38	8.28 ± 0.18	10.96 ± 0.20
R-260	44.18 ± 0.41	4.75 ± 0.15	6.78 ± 0.34	0.08 ± 0.04	<d.l.	8.32 ± 0.39	51.37 ± 0.14	29.95 ± 0.47	18.68 ± 0.25	16.28 ± 0.22

<sup>a</sup> Calculate by difference, O = 100% – C (%) – H (%) – N (%) – S (%) – Cl (%) – A<sub>d</sub> (%); FC = 100% – V<sub>d</sub> – A<sub>d</sub>. <sup>b</sup> "d.l.", detection limit.



Table 2 XRF analysis (only components of ash &gt;0.01 are listed)

XRF	CaO	Cl	Fe <sub>2</sub> O <sub>3</sub>	MgO	Cr <sub>2</sub> O <sub>3</sub>	TiO <sub>2</sub>	PbO	SiO <sub>2</sub>	Na <sub>2</sub> O	MnO	Al <sub>2</sub> O <sub>3</sub>	SO <sub>3</sub>	K <sub>2</sub> O	P <sub>2</sub> O <sub>5</sub>	SrO
wt%	66.45	7.14	5.85	3.01	2.92	1.47	0.87	0.53	0.18	0.13	0.12	0.08	0.06	0.05	0.01

$$\text{Energy density} = \frac{\text{HHV}_i}{\text{HHV}_0} \times 100\% \quad (2)$$

where HHV<sub>0</sub> and HHV<sub>i</sub> represent the high heating values of the raw sample and hydrochar, respectively.

**2.3.2. Fourier-transform infrared spectroscopy.** A Fourier-transform infrared (FTIR) spectrophotometer (Vertex 70, Bruker, Germany) and the KBr particle method were used to determine the major functional groups in the samples. Prior to testing, 0.5 mg + 0.03 mg of sample was weighed and mixed with KBr powder at a mass ratio of 1 : 200. FTIR spectra were recorded with a resolution of 4 cm<sup>-1</sup> in the wavenumber range of 4000 cm<sup>-1</sup> to 400 cm<sup>-1</sup>. The background was removed from each spectrum before analysis.

**2.3.3. <sup>13</sup>C nuclear magnetic resonance (NMR).** The C-containing structures of the unprocessed materials and hydrochars were analyzed using cross-polarized magic angle spin (CP-MAS) and total suppression of sidebands sequence (TOSS) techniques together with <sup>13</sup>C solid-state nuclear magnetic resonance (NMR) (Bruker AVANCE II 500). The following parameters were used: 1000 scans, 5 s cycle delay time, 16.5 μs pulse delay time, 8 kHz rotor rotating speed, 1.5 ms cross-polarization contact time, and 5 kHz magic angle rotation rate. The <sup>13</sup>C NMR spectra were calibrated using Origin software.

## 2.4. Pyrolysis reactivity

The thermal degradation of solid samples was assessed using thermogravimetric (TG) analysis. Each sample was heated at a rate of 20 °C min<sup>-1</sup> from 50 °C to 900 °C. Nitrogen gas (99.99%) flowing at 100 mL min<sup>-1</sup> was used to create an oxygen-free environment for thermal decomposition. To assess how the HTC conditions affected the thermal decomposition behavior,

the pyrolysis curves were used to determine the total loss of mass, initial decomposition temperature (*T*<sub>i</sub>), final decomposition temperature (*T*<sub>f</sub>), maximum weight loss rate ((*dw/dt*)<sub>max</sub>), and mean weight loss rate ((*dw/dt*)<sub>mean</sub>). Furthermore, the pyrolysis reactivity of the hydrochars was quantitatively assessed using the comprehensive pyrolysis index (CPI), as follows:<sup>43,44</sup>

$$\text{CPI} = [(\text{dw/dt})_{\text{max}} \times (\text{dw/dt})_{\text{mean}}] / (T_i \times T_f)$$

## 3. Results and discussion

### 3.1. Hydrochar properties

The chemical structure and thermal stability of a hydrochar are primarily affected by its HTC temperature.<sup>5,28</sup> The hydrochar yields obtained under different HTC temperatures are shown in Fig. 2(a). With increasing HTC temperature from 220 to 260 °C, the hydrochar yield showed a clear downward trend. The RPVC yields were significantly higher at 220 °C and 240 °C than those of SPVC. However, at 260 °C, the SPVC and RPVC yields were nearly equal. Ma *et al.*<sup>28</sup> and Ning *et al.*<sup>5</sup> also noted a similar tendency, reporting that when the HTC temperature exceeded 260 °C, the solid phase yield remained constant even if the temperature was further increased. Lower hydrochar yields are typically caused by the rapid removal of HCl from raw materials.<sup>27</sup> Evidently, RPVC exhibited greater thermal stability during the HTC treatment process than SPVC. This was attributed to the addition of stabilizers and fillers during the production of RPVC.<sup>45,46</sup> The removal of Cl and degradation of the additives in RPVC explains similar yields of both hydrochars at 260 °C. This will be further confirmed by the compositional analysis of the hydrothermal carbons below.

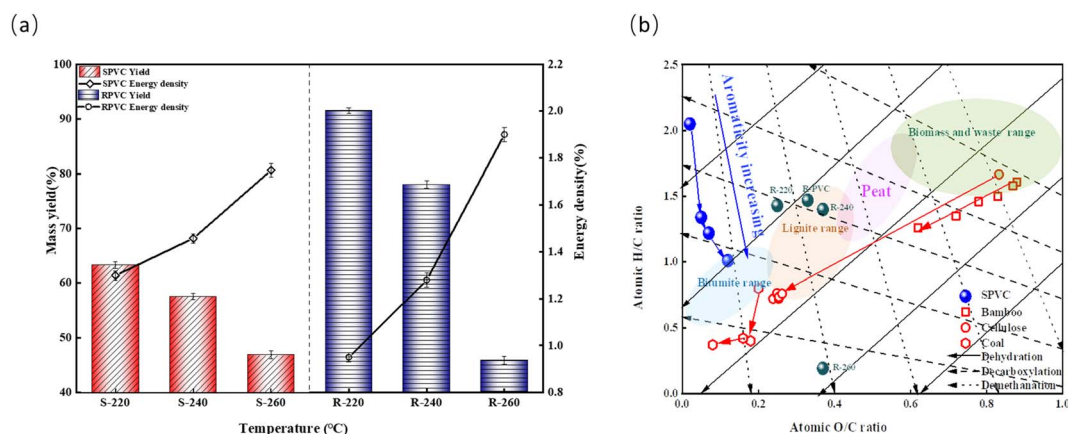


Fig. 2 (a) Yield and energy density of samples under different hydrothermal temperatures. (b) Van-Krevelen diagram.





The energy density of hydrochar significantly increased with increasing HTC temperature, providing further evidence that treating PVC with HTC is an energy-enriching process. This is very beneficial for converting PVC waste into a high-value-added product.

Proximate and ultimate analyses are important methods for determining the organic and chemical composition of fuels. As displayed in Table 1, the majority of SPVC consisted of volatile matter (V), which accounted for 95.07% of this sample. This was followed by fixed carbon (FC), which accounted for 4.94%. No ash (A) was found in SPVC. After the HTC treatment, the V content of the obtained hydrochar sharply decreased to 43.46%. Meanwhile, FC showed a significant increasing trend, from 4.94% in the original SPVC sample to 43.46% with increasing HTC temperature. The decrease in V and the increase in FC indicated the occurrence of devolatilization and carbonation reactions.<sup>47</sup> Due to the excess loss of V during the HTC process, the hydrochars contained higher ash content. These findings are in line with previous studies.<sup>5</sup> The ultimate analysis showed that the carbon content in the hydrochar increased from 39.44% to 79.07% as the temperature increased, gradually approaching that of bituminous coal,<sup>48</sup> while the concentration of Cl drastically decreased from 52.88% to 5.20%. This suggests that the harmful element Cl, which constrains the reuse of PVC, can be removed from PVC and converted into a C-rich carbon-based material at lower temperatures by HTC treatment. Despite the increasing oxygen content of these hydrochars, they still exhibited significantly lower oxygen content than hydrochar made from biomass (16 to 36%)<sup>49,50</sup> and bituminous coal (30% to 37%).<sup>51</sup> For RPVC, as the HTC temperature increased, the ash content decreased. Combined with XRF analysis, this likely indicates that the HCl removed from the RPVC dissolved in the water to form hydrochloric acid, which had the ability to partially dissolve CaCO<sub>3</sub>. This is the main reason for the similar yield of the two hydrochars at 260 °C. Compared to SPVC, the hydrochar prepared using RPVC had much lower C content. Zhuang *et al.*<sup>43</sup> reported similar results with herb tea waste, penicillin mycelial waste, and sewage sludge, all of which had high ash content. It can be speculated that the higher ash content of RPVC prevented this PVC sample from being carbonized as well as SPVC, which would explain why RPVC contained less carbon.

The atomic H/C and O/C ratios of the prepared hydrochars were plotted in a Van-Krevelen diagram to investigate the structural changes during HTC processing. These ratios were compared with those of several coal and hydrochar samples prepared from other solid wastes.<sup>48,52–54</sup> As shown in Fig. 2(b), as the HTC temperature rose, the H/C and O/C ratios of the hydrochar prepared from SPVC shifted toward those of bituminous coal. Compared to other hydrochars, the hydrochar derived from SPVC followed a different coalification process. SPVC primarily underwent dehydration and demethylation, showing no decarbonization. According to a previous study,<sup>27</sup> the degradation of PVC in critical water systems consists of three steps: dehydrochlorination (200–250 °C), polyene formation and initial decomposition (250–350 °C), and further decomposition (350–450 °C). Consequently, SPVC leads a unique reaction path in the Van-Krevelen diagram due to the

efficient elimination of HCl. As a result, the chemical structure and C content of the hydrochar prepared from SPVC shifted toward those of lignite. This indicates the strong potential of using hydrochar instead of traditional fossil fuels. These findings confirm that HTC can be used to produce high-value-added materials with high C content and HHV by upgrading hazardous PVC waste. Because the comparatively high ash content of RPVC inhibited the coalification process during HTC, RPVC and the RPVC-derived hydrochars were excluded from the Van-Krevelen diagram.

## 3.2. Modification of hydrochar structure and mechanism analysis

### 3.2.1. Evolution of surface functionalities.

As depicted in Fig. 3(a), the FTIR spectrum of hydrochar undergoes significant changes with increasing hydrothermal temperature. This indicates that the hydrothermal temperature significantly affected the functional groups of the hydrochars. Characteristic peaks associated with Cl were observed at 2817 cm<sup>-1</sup>, 2969 cm<sup>-1</sup>, 1250 cm<sup>-1</sup>, 1328 cm<sup>-1</sup>, 617 cm<sup>-1</sup>, and 694 cm<sup>-1</sup>. These peaks were attributed to the C–H stretching vibration in –CHCl, the C–H bending in –CHCl–, and C–Cl stretching vibrations. With increasing HTC temperature, these peaks became weaker, and they were almost eliminated at 260 °C.<sup>30,55</sup> These changes indicate that organochlorines were gradually removed from the hydrochar, in agreement with the elemental analysis. Some new chemical bonds appeared in the hydrochar, with peaks located at 1610 cm<sup>-1</sup>, 1700 cm<sup>-1</sup>, 3020 cm<sup>-1</sup>, and 3430 cm<sup>-1</sup> ascribed to conjugated C=C–, the stretching vibration of C=O, the stretching vibration of C–H in –CH=CH–, and the stretching vibration of –OH, respectively.<sup>56</sup> According to previous studies, the dechlorination of PVC is accomplished by substituting –Cl with –OH and eliminating HCl. The HCl elimination reaction and the strong inter- and intra-molecular dehydration reactions during the HTC process led to the formation of C=C and C=O.<sup>25,27,30</sup> This was confirmed by the Van-Krevelen diagram analysis. Apparently, the Cl-containing functional groups in SPVC were converted to C=C, C–O, and C=O functional groups by de-HCl and –OH substitution reactions. The oxygen-containing functional group content of the hydrochar increased after the HTC process compared with the untreated material. This was consistent with another study that investigated the hydrothermal treatment of lignocellulosic biomass.<sup>17</sup> The higher oxygen content of hydrochar is a significant characteristic and means that the use of hydrochar is particularly promising in various fields such as adsorption and catalysis.<sup>57–59</sup> Additionally, methylene group (–CH<sub>2</sub>–) peaks shifted from 2845 cm<sup>-1</sup> and 2910 cm<sup>-1</sup> to 2851 cm<sup>-1</sup> and 2922 cm<sup>-1</sup>, and these peaks gradually became the strongest vibrational peaks of the hydrochar. This peak shift is likely caused by the different natures of the methylene in the original PVC and the aromatic network formed by the transformation of the conjugated double bonds in the dehydrochlorinated PVC.<sup>60</sup> Moreover, the intensity of the absorption peak at 1095 cm<sup>-1</sup> diminished, indicating the thorough destruction of the PVC carbon skeleton. The formation of aromatic structures in these PVC-based hydrochar



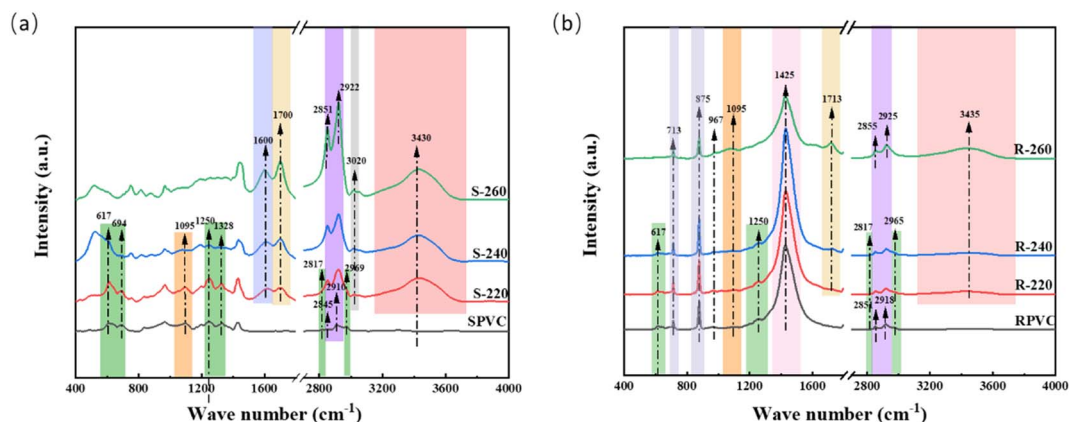


Fig. 3 FTIR spectra of SPVC, RPVC, and hydrochars.

samples was similar to the carbonization process of biomass,<sup>18,61</sup> indicating that significant carbonization reactions occurred within the PVC during HTC.

As shown in Fig. 3(b), the FTIR spectrum of RPVC showed bands at 713 cm<sup>-1</sup> and 875 cm<sup>-1</sup> that were attributed to the in-plane and out-of-plane stretching vibrations of CO<sub>3</sub><sup>2-</sup>.<sup>62</sup> A

composite absorption band centered at 1425 cm<sup>-1</sup> was ascribed to the vibrations of -CH<sub>2</sub> in the PVC, COO in the stabilizer, and the CO<sub>3</sub><sup>2-</sup> in CaCO<sub>3</sub>.<sup>62,63</sup> The higher intensity of the CO<sub>3</sub><sup>2-</sup> peak clearly indicated that RPVC contained a considerable proportion of CaCO<sub>3</sub> filler. The peaks located at 617 cm<sup>-1</sup>, 1250 cm<sup>-1</sup>, 2817 cm<sup>-1</sup>, and 2962 cm<sup>-1</sup> gradually weakened with increasing

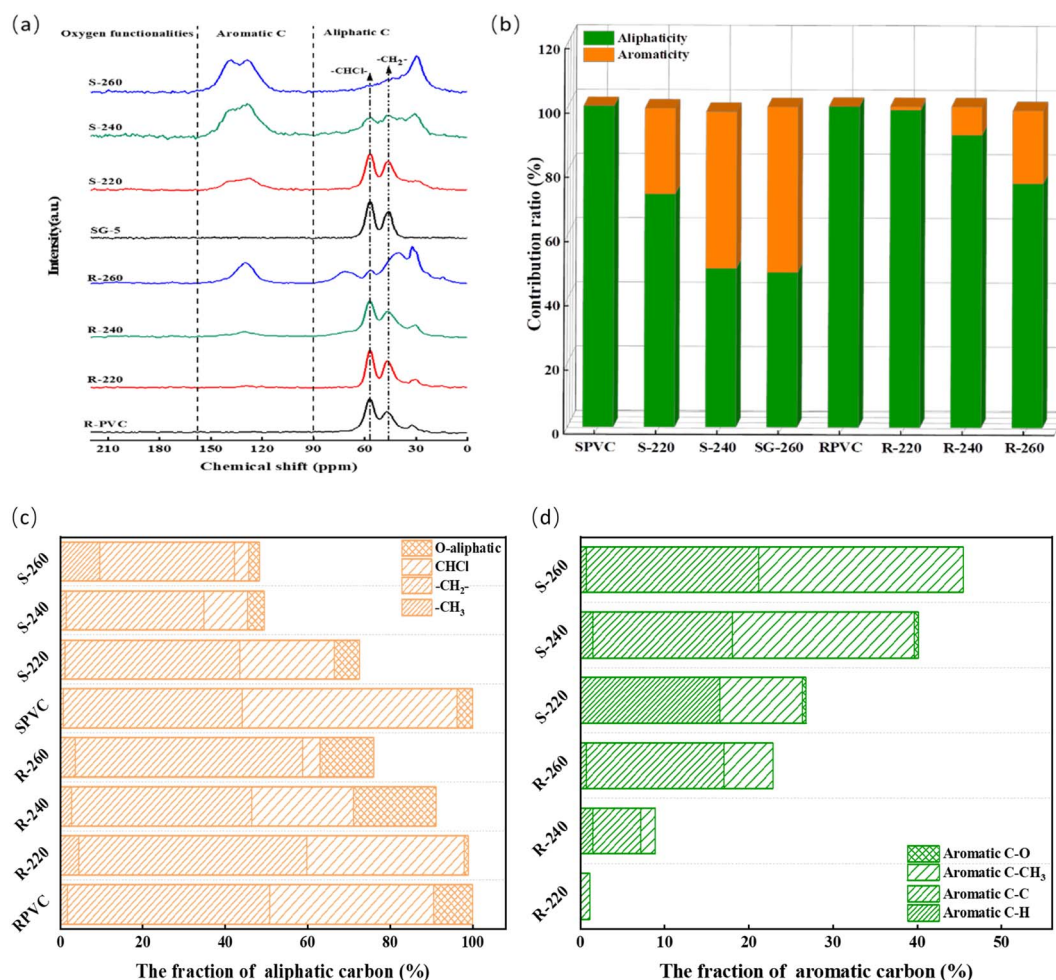


Fig. 4 <sup>13</sup>C NMR spectra of S-PVC, R-PVC, and hydrochars prepared under various HTC temperatures.

HTC temperature. Unexpectedly, no obvious C=C vibrational peaks were observed in the hydrochar prepared from RPVC, and only C=O and -OH peaks were visible. This was potentially due to a change in the path of dechlorination. Typically, the interaction of free radicals and structures with low heat stability in the structure of PVC causes dechlorination.<sup>64</sup> Dehydrochlorination is then triggered by the zipper process, which eliminates the neighboring -H and -Cl atoms to produce conjugated double bonds.<sup>26</sup> However, the presence of a thermal stabilizer and CaCO<sub>3</sub> filler can trap the released HCl and inhibit the autocatalytic PVC degradation reaction, thus hindering the formation of C=C functional groups in hydrochar.<sup>46,65</sup> As a result, it can be speculated that the substitution of -Cl with -OH was the main reason for the thermal degradation of RPVC. Thus, the additives in RPVC influenced its dechlorination process, resulting in the formation of hydrochar with different functional groups. Different dechlorination pathways may lead to the formation of hydrochar with different structures, which will be analyzed in a following study.

**3.2.2. Evolution of carbon skeleton structure.** To analyze the overall structure of the PVC feedstock and the prepared hydrochars, <sup>13</sup>C CPMAS NMR was performed to supplement the FTIR analysis. As shown in Fig. 4(a), the <sup>13</sup>C NMR spectra were divided into three different regions assigned to aliphatic carbon (0–90 ppm), aromatic carbon (90–165 ppm), and carbonyl carbon (165–220 ppm).<sup>30,66</sup> The predominant carbon-containing functional group of SPVC and RPVC was aliphatic carbon (0–90 ppm), and the main peaks located around 46 and 57 ppm were ascribed to the carbon atoms in -CH<sub>2</sub>- and -CHCl, respectively. This is similar to standard PVC.<sup>32</sup> After HTC, the spectra of the hydrochar showed distinct carbon resonance signals in the aromatic region (110–160 ppm). These signals became progressively broader and stronger as the HTC temperature increased, which indicated the formation of a more complex hydrochar structure with aromatic groups. To investigate the impact of the HTC process on the hydrochar structure in more detail, different types of carbon were quantitatively analyzed using the Gaussian peak split method. The structural parameters of hydrochar were calculated and summarized, as shown in Table 3. The signals were assigned based on other literature reports,<sup>49,67</sup> and detailed split-peak fitting is provided in Fig. S1 in the ESI.†

As shown in Fig. 4(b), the aliphaticity of the hydrochar decreased and its aromaticity increased with increasing HTC temperature, indicating that the structure of the hydrochar was transformed from a long aliphatic chain structure to an aromatic structure. The relative C-Cl content in the hydrochar gradually decreased as the HTC temperature increased, indicating that a higher HTC temperature facilitated the breaking of C-Cl bonds, consistent with the FTIR spectra and elemental analysis. For the hydrochar derived from RPVC, the O-aliphatic content substantially increased from 9.43% (raw material) to 20.04% after HTC at 240 °C. However, at 260 °C, the O-aliphatic content decreased to 13.08%. In contrast to RPVC, the O-aliphatic content in the hydrochar derived from SPVC did not significantly vary with HTC temperature (3.76%, 5.99%, 3.97%, and 2.54%). Elimination and substitution reactions are the

Table 3 Structural parameters of samples

Symbol	Structural parameters	Chemical shift and calculation formula	SPVC	S-220	S-240	S-260	RPVC	R-220	R-240	R-260
$f_{al}^M$	Methyl ratio	0–25	0.66%	1.11%	1.40%	9.59%	1.78%	4.45%	2.69%	3.54%
$f_{al}^H$	Methylene ratio	25–50	43.43%	42.39%	33.33%	32.66%	49.01%	55.35%	43.80%	55.20%
$f_{al}^{Cl}$	Chlorine-aliphatic carbon	50–60	52.15%	23.02%	10.72%	3.45%	39.77%	38.15%	34.60%	4.20%
$f_{al}^O$	Oxy-aliphatic carbon	60–90	3.76%	6.00%	3.97%	2.54%	9.43%	0.96%	20.04%	13.08%
$f_{ar}^H$	Protonated aromatic carbon	90–128	—	16.52%	10.20%	6.85%	—	—	1.47%	0.70%
$f_{ar}^B$	Bridged aromatic carbon ratio	128–137	—	—	16.58%	20.49%	—	1.09%	5.69%	16.35%
$f_{ar}^C$	Alkyl-substituted carbon ratio	137–148	—	9.84%	21.60%	24.26%	—	—	1.72%	5.79%
$f_{ar}^O$	Oxygen substituted aromatic carbon	148–165	—	0.45%	0.49%	—	—	—	—	—
$f_{ar}^{COO}$	Carboxylic carbon	165–188	—	—	0.26%	—	—	—	—	0.36%
$f_{ar}^{CO}$	Carbonyl carbon	188–220	—	0.68%	1.43%	0.15%	—	—	—	0.79%
$f_{al}$	Aliphatic carbon ratio	$f_{al} = f_{al}^M + f_{al}^H + f_{al}^{Cl} + f_{al}^O$	100%	72.52%	49.43%	48.25%	100%	98.91%	91.13%	76.02%
$f_{ar}$	Aromatic carbon ratio	$f_{ar} = f_{ar}^H + f_{ar}^B + f_{ar}^C + f_{ar}^O$	—	26.81%	48.72%	51.60%	0	1.09%	8.87%	22.84%
$A_i$	Methylene percentage of aliphatic carbon	$A_i = f_{al}^H/f_{al}$	43.43	58.45	67.44%	67.69%	49.01%	55.96%	48.06%	72.61%
$L$	Average carbon chain length	$L = (f_{al}^H + f_{al}^M)/f_{al}$	66	39	25	4	29	13	17	17
$H_{au}/C_{ar}$	Hydrogen to carbon atom ratio of unsubstituted aromatic ring	$H_{au}/C_{ar} = f_{ar}^H/(f_{ar}^H + f_{ar}^B)$	—	—	0.38	0.25	—	—	0.21	0.04
$X_b$	Aromatic clusters size	$X_b = f_{ar}^H/(f_{ar}^H + f_{ar}^B)$	—	—	0.34	0.40	—	—	0.64	0.72





main cause of PVC dechlorination.<sup>28,41,68</sup> Nagai also reported that dechlorination can be competitive with the nucleophilic substitution of  $-OH$ .<sup>26</sup> This further confirms that the removal of Cl by RPVC mainly occurred through the substitution of  $-Cl$  with  $-OH$  and the conversion of the C–Cl bonds in RPVC to C–O bonds. Increasing the HTC temperature reduced the C–O bonds due to the more intense dehydration and dehydrogenation reaction. For SPVC, the elimination reaction may play a major role in breaking the C–Cl bonds and mainly converting them to C=C bonds, which form conjugated polyenes. Only a small fraction of the C–Cl bonds are converted to C–O with increasing HTC temperature. Additionally, with increasing HTC temperature, the methyl ratio ( $f_{al}^M$ ) and methylene percentage of aliphatic carbon ( $A_i$ ) in hydrochar increased and the average carbon chain length ( $L$ ) decreased for all hydrochar samples except R-220. This indicated that the polymer chains of the original PVC material were broken. Mainly due to the extreme instability of conjugated polyenes, de-HCl PVC randomly fractures at high temperatures to form polyene fragments.<sup>69</sup> A small amount of polyene fragmentation results in aliphatic hydrocarbons, the majority of which undergo molecular rearrangements and cyclization reactions. Cyclic compounds can also be produced by the direct decomposition of polyol.<sup>70,71</sup> Therefore, the aliphatic groups in the hydrochar samples were mainly short-chain paraffins and cycloalkanes.

Conventional fuels contain significant aromatic content. Thus, the composition of the hydrochar aromatic structure was studied to evaluate its potential for subsequent thermal applications.<sup>43</sup> As shown in Fig. 4(c), the aromatic structure of the hydrochar was mainly composed of protonated aromatic carbon, bridged aromatic carbon, and alkyl-substituted carbon. Under a high temperature, the conjugated polyene chains broke and some of the polyene fragments underwent intramolecular rearrangement and cyclization to form monocyclic aromatic hydrocarbons such as benzene and toluene.<sup>69,70</sup> Polyene fragments can also produce fused-ring aromatic compounds such as 2-ring PAHs, 3-ring PAHs, and 4-ring PAHs through the Diels–Alder reaction.<sup>72,73</sup> As the HTC temperature increased, the protonated aromatic carbon ratio decreased, while the bridged aromatic carbon ratio and the condensation degree of the aromatic ring ( $H_{ar}/C_{ar}$ ) increased. An important parameter for estimating the size of aromatic clusters is the molar fraction of aromatic bridgehead carbon ( $X_b$ ).<sup>74</sup> For example, the  $X_b$  value of benzene is 0.20 and that of naphthalene is 0. The calculated  $X_b$  values of S-240, S-260, R-240, and R-260 were 0.34, 0.40, 0.64, and 0.72, respectively. These results indicate that the average number of aromatic rings per cluster was more than 2, and a higher HTC temperature resulted in larger aromatic clusters. Thus, elevating the HTC temperature promoted the polycondensation of aromatic rings, and the size of the aromatic clusters in the hydrochar increased with increasing HTC temperature. Notably, although the hydrochars derived from RPVC had lower aromaticity than the SPVC-derived hydrochars, the R-240 and R-260 samples had aromatic structures with larger aromatic cluster sizes than S-240 and S-260. Karayıldırım *et al.* investigated the thermal degradation of PVC using  $CaCO_3$  as an absorbent and found that  $CaCO_3$  has a significant effect

on the distribution of the thermal degradation products of PVC.<sup>75</sup> Therefore, the presence of the additives in RPVC potentially promoted the polycondensation between aromatic rings. The alkyl-substituted carbon ratio increased with increasing HTC temperature, which was mainly because the higher HTC temperature intensified the breakage of the PVC main chain structure.

### 3.3. Relationship between structural features and thermal reactivity

**3.3.1. Pyrolysis behavior and reactivity.** The structure of a material determines its properties.<sup>76,77</sup> According to the above analyses, the changes to the chemical structure caused by changing the HTC temperature will affect the pyrolysis reactivity of the prepared hydrochars. The TG and DTG curves of RPVC, SPVC, and the hydrochars obtained under various HTC conditions are illustrated in Fig. 5. SPVC and the SPVC-derived hydrochars underwent degradation in two stages, while RPVC and the RPVC-derived hydrochars underwent four degradation stages. The bond dissociation energy of C–Cl bonds is  $326 \text{ kJ mol}^{-1}$ , which is lower than the dissociation energy of C–H bonds ( $347 \text{ kJ mol}^{-1}$ ) and C–C bonds ( $435 \text{ kJ mol}^{-1}$ ).<sup>78–80</sup> Therefore, the first peak on the DTG curve was ascribed to C–Cl bond breakage. With increasing HTC temperature, this first peak significantly decreased and almost completely disappeared in the DTG curve of S-260, confirming that HTC treatment could effectively remove the Cl from PVC. The second peak on the DTG curves increased with increasing HTC temperature, and this peak corresponded to the breakage of C–C bonds. When macromolecular structures are randomly fragmented at high temperatures, aromatic compounds are released.<sup>79,81</sup> Ning *et al.* reported that the aromaticity of hydrochar increases with increasing HTC temperature, which is in agreement with this result.<sup>70</sup> The third and fourth weight loss stages in the RPVC curves corresponded to the degradation of the filler. Wang studied the thermal degradation of PVC films and also observed a similar degradation process.<sup>82</sup> With increasing HTC temperature, the third peak on the DTG curve significantly weakened, and this peak almost completely disappeared in the R-260 curve. On the other hand, the fourth peak was initially enhanced and then weakened with increasing HTC temperature. This was because the heat stabilizers, smoke inhibitors, and  $CaCO_3$  fillers in RPVC had an inhibitory effect on the dechlorinated HCl.<sup>68,83</sup> Qi *et al.* also reported that heat stabilizers in a urine sample collection limited dichlorination.<sup>84</sup> Apparently, the additives in RPVC were involved in the hydrothermal degradation reaction of RPVC, resulting in a change in its composition.

The pyrolysis parameters of PVC and the prepared hydrochars are shown in Table 4. The initial temperature ( $T_i$ ) of the hydrochars (except for R-260) decreased with increasing hydrothermal temperature. For R-260, the value of  $T_i$  increased with increasing temperature. It has been reported that the presence of defective structures (such as allyl chloride) in hydrochars leads to a decrease in the  $T_i$  value.<sup>11</sup> During the HTC process, C–Cl bonds were converted to C–O bonds, C=O bonds,



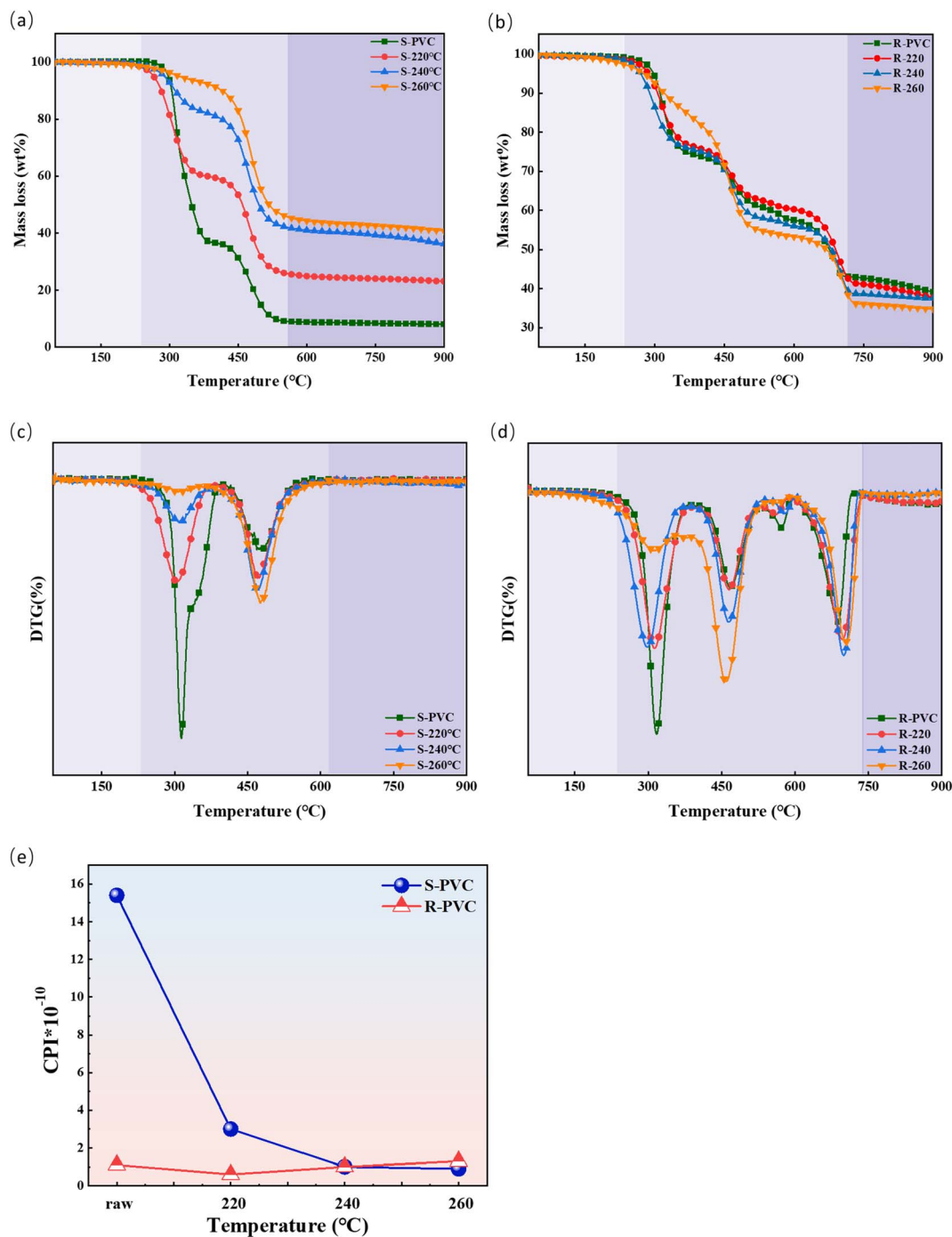


Fig. 5 TG-DTG curves and pyrolysis reactivity of SPVC, RPVC, and hydrochars.

Table 4 The pyrolysis characteristic parameters of raw and hydrochar

Characteristic parameters	SPVC	S-220	S-240	S-260	RPVC	R-220	R-240	R-260
Weight loss at 900 °C	92.0	76.9	63.7	55.8	59.3	58.9	62.2	64.9
$T_i$ [°C]	295.7	259.8	275.4	343.5	287	276.3	285.7	253.7
$T_f$ [°C]	508.3	630.7	851.4	819.5	761.5	831.5	730.2	735.3
$(dw/dt)_{max}$ [% per s]	1.39	0.55	0.59	0.67	0.52	0.34	0.33	0.41
$(dw/dt)_{mean}$ [% per s]	0.13	0.06	0.03	0.04	0.04	0.03	0.04	0.04



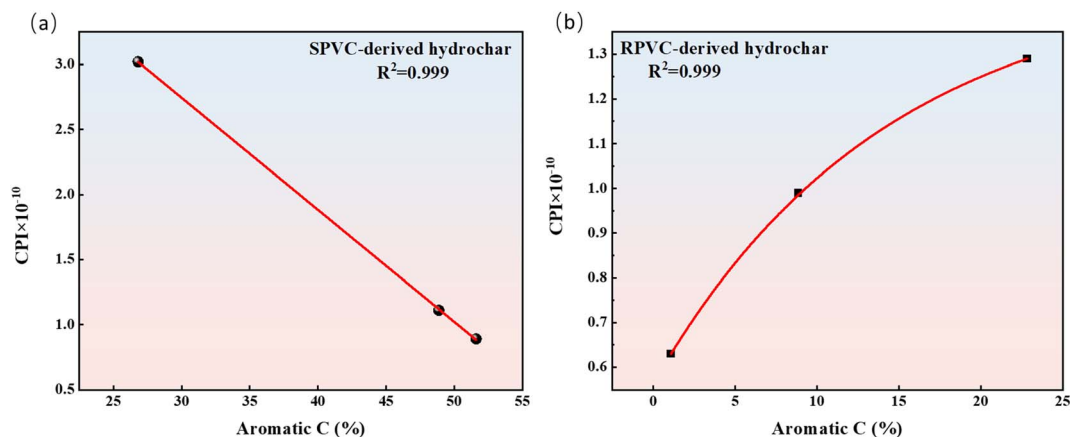


Fig. 6 Relationship between CPI and aromaticity of hydrochars.

and C=C bonds, which enhanced the thermal stability of the hydrochar and increased its  $T_i$  value. The hydrochars had significantly higher pyrolysis temperatures ( $T_f$ ) and lower mean loss rates ( $(dw/dt)_{\text{mean}}$ ) than the untreated PVC feedstock. This was potentially due to the reduction of the low-energy C-Cl bond and the formation of an aromatic structure. Therefore, the hydrochar samples exhibited enhanced thermal stability compared to the raw PVC materials. Therefore, in addition to effectively reducing the chlorine content in hydrochar, hydrothermal carbonization can significantly improve the thermal stability of the raw material, which is consistent with previous studies on biotite hydrothermal carbonization.<sup>18,61</sup> This improved thermal stability is highly significant for the storage and transportation of hydrochar.

The comprehensive pyrolysis index (CPI) was adopted to quantitatively describe the reactivity of the hydrochar during pyrolysis. A higher CPI typically denotes a quick and simple progression of the pyrolysis reaction, while a lower CPI indicates the opposite. As shown in Fig. 5, the CPI values of the hydrochars derived from SPVC substantially decreased from  $1.54 \times 10^{-9}$  (SPVC) to  $8.94 \times 10^{-11}$  (S-260). However, the effect of HTC temperature on the CPI values of the hydrochars derived from SPVC was not significant. With increasing HTC temperature, these CPI values ranged from  $6.25 \times 10^{-11}$  to  $1.29 \times 10^{-10}$ . The thermal reactivity of hydrochar is mainly affected by the hydrochar structure and components.<sup>85–87</sup> On one hand, the high relative ratio of aromaticity to aliphaticity negatively affects the pyrolysis reactivity.<sup>88</sup> On the other hand, high oxygen-containing functional group content means a relatively reactive macromolecule network.<sup>89</sup> In addition, the residual additives in hydrochar also have a significant effect on the thermal degradation process.<sup>45,90</sup> Therefore, structure and additives both influence the reactivity of hydrochar pyrolysis. The relationship between the structural characteristics and pyrolytic reactivity of the prepared hydrochars is discussed in detail in the next section.

### 3.3.2. Structure–reactivity relationship for pyrolysis.

Establishing the relationship between the molecular structure and reactivity of hydrothermal carbon is essential for further understanding the thermal degradation mechanism

of PVC. Analyzing molecular structures can provide insight into the thermal reactivity of hydrothermal products.<sup>37,38,91</sup> Thus, the reactivity of the pyrolysis reaction is essentially related to the aromatic structure of fuel.<sup>39,47</sup> As shown in Fig. 6, the CPI values and variation in aromaticity (obtained by  $^{13}\text{C}$  NMR analysis) clearly show a structure–reactivity relationship. The CPI values of the hydrochars prepared from SPVC were negatively correlated with aromaticity. These CPI values monotonically decreased with increasing aromaticity, and the linear correlation coefficient ( $R^2$ ) was 0.999. However, the CPI values of the hydrochars prepared from RPVC exponentially increased with increasing aromaticity. For SPVC, low-energy chemical bond breakage to remove a volatile fraction (HCl) improved the thermal stability of the hydrochar. Moreover, the cyclization and aromatization reactions were intensified with increasing HTC temperature, and the small molecule intermediates formed during hydrolysis underwent polymerization reactions and formed large aromatic clusters. Zhuang *et al.* also reported that the CPI values of coals, herb tea waste, and penicillin mycelial waste linearly decreased with increasing aromaticity.<sup>43</sup> Thus, HTC treatment significantly reduced the chlorine content in the PVC and shifted the structure and physicochemical properties of the PVC toward higher-order fuels. This structure–reactivity model can be used to initially predict the thermal reactivity of hydrochar. For RPVC, the distinct changes in the RPVC-derived hydrochars can be attributed to three factors. One, the residual additives in the PVC lowered the pyrolysis temperature during thermal decomposition, curbing the formation of polyene structures and facilitating the release of volatiles.<sup>46,90,92</sup> Two, the structure of RPVC was only partially altered by the HTC treatment. Three, the additives in the PVC reacted with PVC degradation intermediates, which generated novel substances within the hydrothermal carbon. Hence, the trend in the RPVC hydrochar reactivity can be attributed to the combined effects of hydrothermal carbonization and additive interaction. Clearly, the large amount of filler in RPVC weakened the effect of the hydrochar structure on pyrolytic reactivity. This is of great concern in practical applications.

## 4. Conclusion

In this study, the structural changes in PVC materials following HTC treatment and the pyrolysis reactivity of the resulting hydrochar were evaluated. With increasing HTC temperature, the hydrochar yield decreased, the hydrochar became more enriched with C, the Cl content significantly decreased, the energy density increased, and the H/C and O/C ratios approached those of bituminous coal. Additionally, the structure of the PVC raw materials was converted to a coal-like structure, with a transformation from long straight chains to short-chain paraffins, cycloalkanes, and aromatics structures occurring as the HTC temperature increased. Moreover, increasing the HTC temperature led to the formation of aromatic structures with a high degree of polymerization. The additives in RPVC had a significant inhibitory effect on the dechlorination of this PVC material during hydrothermal carbonization. However, the additives also promoted a condensation reaction between aromatic rings, leading to the formation of a hydrochar with a different structure than that of SPVC-derived hydrochar. Both the thermal degradation behavior and thermal reactivity of the hydrochar varied with increasing hydrothermal temperature. For SPVC, the total mass loss and the CPI of hydrochar samples were negatively correlated with HTC temperature, while the CPI decreased as aromatic structures evolved. For RPVC, the total mass loss of pyrolysis was positively correlated with HTC temperature, and the CPI increased with aromatic structure evolution. The effect of the additives in RPVC on pyrolysis was greater than the effect of the hydrochar structure on the pyrolysis process. This work offers insight into the application of hydrothermal carbon prepared using PVC waste and provides a reference for the design, optimization, and scale-up of the thermochemical utilization of PVC waste. The additives in PVC are an important factor affecting the structure, thermal degradation behavior, and pyrolytic reactivity of hydrochar. Therefore, more attention needs to be paid to the effect of additives in real PVC solid waste on the structure and properties of hydrothermal carbon in subsequent PVC hydrothermal carbonization studies.

## Author contributions

Ling Zhang: investigation, data curation, writing – original draft. Qing Wang: funding acquisition, conceptualization. Xingfa Xu: methodology, formal analysis. Zhenye Wang: investigation, writing – review & editing.

## Conflicts of interest

There are no conflicts to declare.

## References

- 1 K. Lewandowski and K. Skórczewska, *Polymers*, 2022, **14**, 3035.
- 2 P. Lieberzeit, D. Bekchanov and M. Mukhamediev, *Polym. Adv. Technol.*, 2022, **33**, 1–12.
- 3 P. Lu, Q. Huang, A. C. T. Bourtsalas, N. J. Themelis, Y. Chi and J. Yan, *J. Environ. Sci.*, 2019, **78**, 13–28.
- 4 Y. Liu, C. Zhou, F. Li, H. Liu and J. Yang, *Resour., Conserv. Recycl.*, 2020, **154**, 104584.
- 5 X. Ning, H. Teng, G. Wang, J. Zhang, N. Zhang, C. Huang and C. Wang, *Fuel*, 2020, **270**, 117526.
- 6 G. Gandon-Ros, A. Soler, I. Aracil and M. F. Gómez-Rico, *Waste Manage.*, 2020, **102**, 204–211.
- 7 X. Zhao, B. Boruah, K. F. Chin, M. Đokić, J. M. Modak and H. S. Soo, *Adv. Mater.*, 2021, 2100843.
- 8 L. Lu, W. Li, Y. Cheng and M. Liu, *Waste Manage.*, 2023, **166**, 245–258.
- 9 P. A. Kots, B. C. Vance, C. M. Quinn, C. Wang and D. G. Vlachos, *Nat. Sustain.*, 2023, DOI: [10.1038/s41893-023-01147-z](https://doi.org/10.1038/s41893-023-01147-z).
- 10 M. S. Qureshi, A. Oasmaa, H. Pihkola, I. Deviatkin, A. Tenhunen, J. Mannila, H. Minkkinen, M. Pohjakallio and J. Laine-Ylijoki, *J. Anal. Appl. Pyrolysis*, 2020, **152**, 104804.
- 11 J. Yu, L. Sun, C. Ma, Y. Qiao and H. Yao, *Waste Manage.*, 2016, **48**, 300–314.
- 12 B. Gui, Y. Qiao, D. Wan, S. Liu, Z. Han, H. Yao and M. Xu, *Proc. Combust. Inst.*, 2013, **34**, 2321–2329.
- 13 J. Zhou, G. Liu, S. Wang, H. Zhang and F. Xu, *J. Energy Inst.*, 2020, **93**, 2362–2370.
- 14 X. Zhou, P. He, W. Peng, S. Yi, F. Lü, L. Shao and H. Zhang, *J. Hazard. Mater.*, 2022, **427**, 128210.
- 15 M. Xu, C. Cao, H. Hu, Y. Ren, G. Guo, L. Gong, J. Zhang, T. Zhang and H. Yao, *Fuel*, 2022, **327**, 125082.
- 16 Y. Shen, R. Zhao, J. Wang, X. Chen, X. Ge and M. Chen, *Waste Manage.*, 2016, **49**, 287–303.
- 17 S. Yu, X. Yang, Q. Li, Y. Zhang and H. Zhou, *Green Energy Environ.*, 2023, **8**, 1216–1227.
- 18 S. Yu, P. Zhao, X. Yang, Q. Li, B. A. Mohamed, J. M. Saad, Y. Zhang and H. Zhou, *J. Anal. Appl. Pyrolysis*, 2022, **166**, 105627.
- 19 S. Wu, Q. Wang, M. Fang, D. Wu, D. Cui, S. Pan, J. Bai, F. Xu and Z. Wang, *Sci. Total Environ.*, 2023, **897**, 165327.
- 20 C. W. Z. Z. Ruikun Wang and Q. Jin, *Energy*, 2019, **186**, 115848.
- 21 H. Liu, I. A. Basar, A. Nzihou and C. Eskicioglu, *Water Res.*, 2021, **199**, 117186.
- 22 L. Zhang, Q. Wang, F. Xu, Z. Wang and G. Zhang, *J. Energy Inst.*, 2022, **105**, 323–333.
- 23 M. Ling, D. Ma, X. Hu, Z. Liu, D. Wang and Q. Feng, *Chemosphere*, 2023, **316**, 137718.
- 24 F. Yang, X. Liu, M. Li, C. Uguna, W. Wang and C. Sun, *Renewable Sustainable Energy Rev.*, 2023, **180**, 113279.
- 25 J. Poerschmann, B. Weiner, S. Wosizdlo, R. Koehler and F. D. Kopinke, *Chemosphere*, 2015, **119**, 682–689.
- 26 Y. Nagai, R. L. Smith, H. Inomata and K. Arai, *J. Appl. Polym. Sci.*, 2007, **106**, 1075–1086.
- 27 Y. Takeshita, K. Kato, K. Takahashi, Y. Sato and S. Nishi, *J. Supercrit. Fluids*, 2004, **31**, 185–193.
- 28 D. Ma, L. Liang, E. Hu, H. Chen, D. Wang, C. He and Q. Feng, *Process Saf. Environ. Prot.*, 2021, **146**, 108–117.



- 29 P. Zhao, T. Li, W. Yan and L. Yuan, *Environ. Technol.*, 2018, **39**, 977–985.
- 30 P. Zhao, Z. Li, T. Li, W. Yan and S. Ge, *J. Cleaner Prod.*, 2017, **152**, 38–46.
- 31 Y. Wang, K. Wu, Q. Liu and H. Zhang, *Process Saf. Environ. Prot.*, 2021, **149**, 105–114.
- 32 Z. Yao and X. Ma, *Energy*, 2017, **141**, 1156–1165.
- 33 C. Lin, P. Zhao, Y. Ding, X. Cui, F. Liu, C. Wang and Q. Guo, *Fuel Process. Technol.*, 2021, **222**, 106959.
- 34 P. Zhao, C. Lin, Y. Li, S. Wu, X. Cui, Y. Ding, F. Liu and Q. Guo, *J. Cleaner Prod.*, 2021, **329**, 129769.
- 35 A. Soler, J. Conesa and N. Ortuño, *Energies*, 2018, **11**, 2612.
- 36 T. Li, P. Zhao, M. Lei and Z. Li, *Appl. Sci.*, 2017, **7**, 256.
- 37 Y. Fan, L. Li, N. Tippayawong, S. Xia, F. Cao, X. Yang, A. Zheng, Z. Zhao and H. Li, *Energy*, 2019, **188**, 116119.
- 38 I. Hita, H. J. Heeres and P. J. Deuss, *Bioresour. Technol.*, 2018, **267**, 93–101.
- 39 H. Takagi, T. Isoda, K. Kusakabe and S. Morooka, *Energy Fuels*, 2000, **14**, 646–653.
- 40 M. Yang, P. Zhao, X. Cui, F. Geng and Q. Guo, *Environ. Technol. Innovation*, 2021, **23**, 101703.
- 41 D. Ma, Q. Feng, B. Chen, X. Cheng, K. Chen and J. Li, *J. Hazard. Mater.*, 2019, **380**, 120847.
- 42 Z. Yao and X. Ma, *Bioresour. Technol.*, 2018, **247**, 302–309.
- 43 X. Zhuang, H. Zhan, Y. Song, X. Yin and C. Wu, *Energy Convers. Manage.*, 2019, **199**, 112014.
- 44 J. Z. X. H. Guangwei Wang, *Bioresour. Technol.*, 2015, **177**, 66–73.
- 45 Y. Lu, B. Wang, M. Xue and Y. Lu, *Waste Manage.*, 2021, **121**, 52–58.
- 46 T. Karayildirim, J. Yanik, M. Yuksel, M. Saglam, C. Vasile and H. Bockhorn, *J. Anal. Appl. Pyrolysis*, 2006, **75**, 112–119.
- 47 L. Li, Y. Huang, D. Zhang, A. Zheng, Z. Zhao, M. Xia and H. Li, *ACS Sustainable Chem. Eng.*, 2018, **6**, 6008–6017.
- 48 N. Ul Saqib, A. K. Sarmah and S. Baroutian, *Waste Manage.*, 2019, **89**, 236–246.
- 49 X. Zhuang, H. Zhan, Y. Song, C. He, Y. Huang, X. Yin and C. Wu, *Fuel*, 2019, **236**, 960–974.
- 50 X. Dong, S. Guo, H. Wang, Z. Wang and X. Gao, *Biomass Convers. Biorefin.*, 2019, **9**, 531–540.
- 51 Q. Wang, Y. Liu, F. Xu, Q. Liu and D. Cui, *J. Therm. Anal. Calorim.*, 2019, **136**, 1631–1643.
- 52 M. Sevilla and A. B. Fuertes, *Carbon*, 2009, **47**, 2281–2289.
- 53 W. Yang, H. Wang, M. Zhang, J. Zhu, J. Zhou and S. Wu, *Bioresour. Technol.*, 2016, **205**, 199–204.
- 54 Y. Lin, X. Ma, X. Peng and Z. Yu, *Waste Manage. Res.*, 2017, **35**, 92–100.
- 55 P. P. R. Cruz, L. C. Silva, R. A. Fiuza Jr and H. Polli, *J. Appl. Polym. Sci.*, 2021, **138**, 50598.
- 56 F. Xiu, Y. Wang, X. Yu, Y. Li, Y. Lu, K. Zhou, J. He, Z. Song and X. Gao, *Sci. Total Environ.*, 2020, **708**, 134532.
- 57 X. Li, J. Hayashi and C. Li, *Fuel*, 2006, **85**, 1700–1707.
- 58 Z. Zhang, Z. Zhu, B. Shen and L. Liu, *Energy*, 2019, **171**, 581–598.
- 59 J. Deng, X. Li, X. Wei, Y. Liu, J. Liang, B. Song, Y. Shao and W. Huang, *Chem. Eng. J.*, 2020, **387**, 124097.
- 60 D. Torres, Y. Jiang, D. A. Sanchez Monsalve and G. A. Leeke, *J. Environ. Chem. Eng.*, 2021, **9**, 104920.
- 61 S. Yu, M. Xie, Q. Li, Y. Zhang and H. Zhou, *J. Energy Inst.*, 2022, **103**, 147–153.
- 62 H. Jemii, D. Hammiche, A. Boubakri, N. Haddar and N. Guermazi, *J. Thermoplast. Compos. Mater.*, 2020, 323151144.
- 63 M. J. Plater, B. De Silva, T. Gelbrich, M. B. Hursthouse, C. L. Higgitt and D. R. Saunders, *Polyhedron*, 2003, **22**, 3171–3179.
- 64 W. H. Starnes and X. Ge, *Macromolecules*, 2004, **37**, 352–359.
- 65 F. Ye, X. Guo, H. Zhan, J. Lin, W. Lou, X. Ma and X. Wang, *Polym. Degrad. Stab.*, 2018, **156**, 193–201.
- 66 C. He, J. Zhao, Y. Yang and J. Wang, *Bioresour. Technol.*, 2016, **211**, 486–493.
- 67 J. Fu, L. Bai, M. Chi, X. Xu, Z. Chen and K. Yu, *J. Environ. Chem. Eng.*, 2022, **10**, 107184.
- 68 Y. Qi, J. He, F. Xiu, W. Nie and M. Chen, *J. Cleaner Prod.*, 2018, **196**, 331–339.
- 69 J. Zhou, B. Gui, Y. Qiao, J. Zhang, W. Wang, H. Yao, Y. Yu and M. Xu, *Fuel*, 2016, **166**, 526–532.
- 70 B. D. H. H. Ning Dong A, *J. Anal. Appl. Pyrolysis*, 2022, **169**, 105817.
- 71 M. I. H. Khan, M. Rana, T. Nshizirungu, Y. T. Jo and J. Park, *ACS Sustainable Chem. Eng.*, 2022, **10**, 2368–2379.
- 72 Y. Ren, C. Cao, H. Hu, S. Lei, X. Yuan, X. Li and H. Yao, *Fuel*, 2022, **317**, 123573.
- 73 T. Lee, J. Oh, T. Kim, D. C. W. Tsang, K. Kim, J. Lee and E. E. Kwon, *Energy Convers. Manage.*, 2018, **164**, 453–459.
- 74 Q. Wang, Y. Hou, W. Wu, M. Niu, S. Ren and Z. Liu, *Fuel*, 2017, **209**, 35–42.
- 75 T. Karayildirim, J. Yanik, M. Yuksel, M. Saglam and M. Haussmann, *J. Polym. Environ.*, 2005, **13**, 365–374.
- 76 Q. He, C. Cheng, A. Raheem, L. Ding, S. Shiung Lam and G. Yu, *Fuel*, 2022, **330**, 125586.
- 77 Q. He, A. Raheem, L. Ding, J. Xu, C. Cheng and G. Yu, *Energy Convers. Manage.*, 2021, **243**, 114383.
- 78 A. López, I. de Marco, B. M. Caballero, M. F. Laresgoiti and A. Adrados, *Fuel Process. Technol.*, 2011, **92**, 253–260.
- 79 H. M. Zhu, X. G. Jiang, J. H. Yan, Y. Chi and K. F. Cen, *J. Anal. Appl. Pyrolysis*, 2008, **82**, 1–9.
- 80 T. Bhaskar, M. Tanabe, A. Muto, Y. Sakata, C. Liu, M. Chen and C. C. Chao, *Polym. Degrad. Stab.*, 2005, **89**, 38–42.
- 81 J. Wu, T. Chen, X. Luo, D. Han, Z. Wang and J. Wu, *Waste Manage.*, 2014, **34**, 676–682.
- 82 G. Wang, H. Zhang, J. Wang and Q. Xue, *J. Iron Steel Res. Int.*, 2022, DOI: [10.1007/s42243-022-00746-y](https://doi.org/10.1007/s42243-022-00746-y).
- 83 S. Kim, *Waste Manage.*, 2001, **21**, 609–616.
- 84 Y. Qi, J. He, Y. Li, X. Yu, F. Xiu, Y. Deng and X. Gao, *Waste Manage.*, 2018, **80**, 1–9.
- 85 X. Zhuang, Y. Song, H. Zhan, X. Yin and C. Wu, *Fuel Process. Technol.*, 2020, **199**, 106304.
- 86 P. Liu, D. Zhang, L. Wang, Y. Zhou, T. Pan and X. Lu, *Appl. Energy*, 2016, **163**, 254–262.
- 87 S. Wang, G. Dai, B. Ru, Y. Zhao, X. Wang, J. Zhou, Z. Luo and K. Cen, *Bioresour. Technol.*, 2016, **218**, 1106–1114.





- 88 X. Zheng, W. Chen, Z. Ying, Z. Jiang, Y. Ye, B. Wang, Y. Feng and B. Dou, *Energy Fuels*, 2020, **34**, 1965–1976.
- 89 Y. Zhao, L. Liu, P. Qiu, X. Xie, X. Chen, D. Lin and S. Sun, *Fuel Process. Technol.*, 2017, **155**, 144–152.
- 90 T. Meng, H. Zhang, F. Lü, L. Shao and P. He, *J. Anal. Appl. Pyrolysis*, 2021, **159**, 105312.
- 91 R. Chen, S. Yuan, X. Wang, X. Dai, Y. Guo, C. Li, H. Wu and B. Dong, *Energy*, 2023, **266**, 126330.
- 92 M. Ji, L. Chen, J. Que, L. Zheng, Z. Chen and Z. Wu, *Process Saf. Environ. Prot.*, 2020, **140**, 211–220.

